

Adhesion patterns in early cell spreading

This article has been downloaded from IOPscience. Please scroll down to see the full text article.

2010 J. Phys.: Condens. Matter 22 194106

(<http://iopscience.iop.org/0953-8984/22/19/194106>)

View [the table of contents for this issue](#), or go to the [journal homepage](#) for more

Download details:

IP Address: 129.252.86.83

The article was downloaded on 30/05/2010 at 08:02

Please note that [terms and conditions apply](#).

Adhesion patterns in early cell spreading

Pavel Ryzhkov¹, Marcus Prass¹, Meike Gummich,
Jac-Simon Kühn, Christina Oettmeier and
Hans-Günther Döbereiner

Institut für Biophysik, Universität Bremen, D-28334 Bremen, Germany

E-mail: hgd@uni-bremen.de


Received 2 October 2009, in final form 21 December 2009

Published 26 April 2010

Online at stacks.iop.org/JPhysCM/22/194106

Abstract

Mouse embryonic fibroblasts explore the chemical suitability before spreading on a given substrate. We find this early phase of cell spreading to be characterized by transient adhesion patches with a typical mean size of $(1.0 \pm 0.4) \mu\text{m}$ and a lifetime of $(33 \pm 12) \text{s}$. Eventually, these patches fuse to initiate extensive spreading of the cell. We monitor cell adhesion using reflection interference contrast and total internal reflection fluorescence microscopy. Digital time lapse movies are analysed employing spatio-temporal correlation functions of adhesion patterns. Correlation length and time can be scaled to obtain a master curve at the fusion point.

 Online supplementary data available from stacks.iop.org/JPhysCM/22/194106/mmedia

(Some figures in this article are in colour only in the electronic version)

1. Introduction

The functional behavior of cells is determined by their chemical and physical interactions with the environment [1]. These external signals from the environment are processed by an internal protein network. Depending on conditions, cells differentiate into a specific cell type, fulfil a certain task or decide to undergo apoptosis if appropriate. In order to gather environmental cues, cell spreading seems to be organized into a sequence of distinct phases of motility [2] differing in growth characteristics of adhesion area and spatio-temporal correlations of the leading membrane edge [2–7]. Briefly, we propose that spreading cells first test the chemical suitability of the substrate in a basal phase (P0), then establish most of the final adhesion area in a continuous spreading phase (P1) and, finally, probe the elastic properties of the substrate in a periodic-contraction phase (P2). All these phases are characterized by a spatially continuous adhesion area. In this work, we revisit the basal phase and show that spreading starts with transient, spatially discontinuous patches of adhesion.

In recent years new analysis tools for cell motility became available [3, 7, 8] allowing cell motility data to be analysed with high spatial and temporal resolution. Focusing on leading edge dynamics and actin flow patterns these tools gave new insights into the motility mechanism from a

systematic, integrated analysis of large amounts of data. In cell adhesion, one line of impetus had been on the dynamics of focal complexes [9], adhesion site formation [10] and force sensing [11–13]. A number of theoretical work addressed these topics [14, 15]. Significant progress has been made with mimetic systems of cell adhesion utilizing giant vesicles [16]. These studies covered topics from non-specific to specific adhesion, and force sensing, i.e. adhesion under force.

Most of the work found in the literature focused on the late stages of adhesion. Few studies have addressed the early stage of cell spreading [7, 17–21]. It is the events at early times that are the focus of this work. Such an approach is advantageous from a physical viewpoint on cell motility, since at early times relatively few signaling pathways are activated. This is in sharp contrast to late stages of cell motility where hundreds of proteins are involved in the formation and control of focal adhesions².

2. Materials and methods

2.1. Cell and substrate preparation

Mouse embryonic fibroblasts (RPTP $\alpha^{+/+}$) [22] were cultured in Dulbecco's MEM medium containing 10% fetal calf

¹ These authors contributed equally to the work.

² For a nearly comprehensive list reflecting current knowledge see www.adhesome.org.

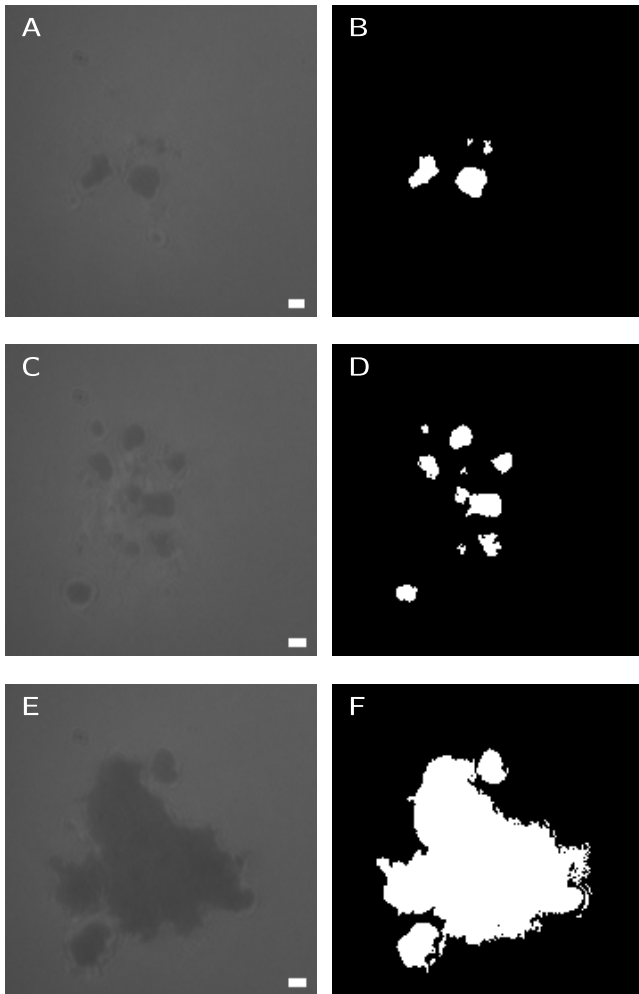


Figure 1. Original images ((A), (C), (E)) and corresponding inverted thresholds ((B), (D), (F)) of RICM micrographs at various stages of cell spreading. Snapshots were taken at time points 134, 246 and 453 s with respect to the start of the movie (available at stacks.iop.org/JPhysCM/22/194106/mmedia).

serum, 0.5% HEPES buffer (pH 6.8–8.2) and 1% of P/S (penicillin/streptomycin).

Prior to the experiment, cells were replated and grown overnight in a culture medium lacking serum. Starving induced an isotropic spreading mode in most of the cells (70%) [3]. Cell spreading essays were performed on fibronectin-coated glass slides. Coating was achieved by immersing slides in $10 \mu\text{g ml}^{-1}$ fibronectin solution for at least 20 min immediately before running the experiment. Microscopic observations were performed with cells immersed in the full medium.

2.2. Reflection interference contrast (RIC) and image analysis

Cell spreading was observed using reflection interference contrast microscopy (RICM) on a Zeiss Axiovert 100TV with the standard oil $63\times$ objective. We recorded 8-bit digital time lapse movies with a temporal and spatial resolution of 1 s/frame and 117 nm/pixel. Areas of close contact of the cells with the substrate were identified as dark patches surrounded

by Newton interference fringes. For further analysis movies were corrected for uneven illumination, thresholded and finally inverted. Thus, the overall outcome was a temporal sequence of binary images with white areas corresponding to cells in contact with the substrate. In figure 1, we show a few examples of this process.

2.3. Total internal reflection fluorescence (TIRF)

We used total reflection interference contrast microscopy on a Zeiss Observer equipped with a TIRF III system as a second technique to monitor adhesion patches. The cellular membrane was labeled with the fluorescent dye DiI (Invitrogen/Molecular Probes), an amphiphilic dialkylcarbocyanine probe which possesses a lipophilic aliphatic tail that inserts into the membrane as well as a charged fluorophore that localizes the probe at the membrane's surface. DiI has an absorption maximum at 549 nm and a fluorescence emission maximum at 565 nm. We used a 488 nm sapphire laser line (coherent) for excitation. The fluorophore was added to the cell solution and incubated for about 20 min at 37°C . Cells were then repeatedly centrifuged and washed with normal, nutrient-containing medium to remove excess dye. Further experimental procedures were as discussed.

TIRF microscopy contrasts only fluorescent structures within the first few hundred nanometres from the interface depending on the exponential decay length of the evanescent wave used for fluorophore excitation:

$$d_\lambda(\epsilon, \epsilon_c) = \frac{\lambda}{4\pi n_1 \sqrt{\sin^2 \epsilon - \sin^2 \epsilon_c}}. \quad (1)$$

Here λ is the wavelength, n_1 the refractive index of the denser medium, ϵ the incident angle and ϵ_c the critical angle beyond which total reflection occurs [23]. It is given by $\sin \epsilon_c = n_2/n_1$, where n_2 is the refractive index of the optically thinner medium. For the glass–water interface ($n_1 = 1.523$, $n_2 = 1.33$), we have $\epsilon_c = 60.8^\circ$. The TIRF III system from Zeiss allows us to quantitatively and reproducibly set the decay length by adjusting the incident angle ϵ , which can be used to fine tune the thickness of the fluorescent layer seen.

2.4. Correlation functions

Contact patterns were characterized by calculating spatio-temporal intensity–intensity correlation functions of the thresholded movies:

$$c(\Delta x, \Delta y, \Delta t) = \frac{\sum_{x,y,t} I(x, y, t) I(x + \Delta x, y + \Delta y, t + \Delta t)}{\sum_{x,y,t} I(x, y, t) I(x, y, t)} \quad (2)$$

where the summation runs over all intensity pairs at the available space and time points separated by $(\Delta x, \Delta y, \Delta t)$. The correlation function has the symmetries $c(\Delta x, \Delta y, \Delta t) = c(-\Delta x, -\Delta y, \Delta t)$ and $c(\Delta x, \Delta y, \Delta t) = c(\Delta x, \Delta y, -\Delta t)$. Thus it was sufficient to calculate $c^+ = c(|\Delta x|, |\Delta y|, |\Delta t|)$ and $c^- = c(-|\Delta x|, |\Delta y|, |\Delta t|)$ separately in order to obtain the full correlation function. Usually, acquired datasets were not large enough to achieve a satisfactory two-dimensional

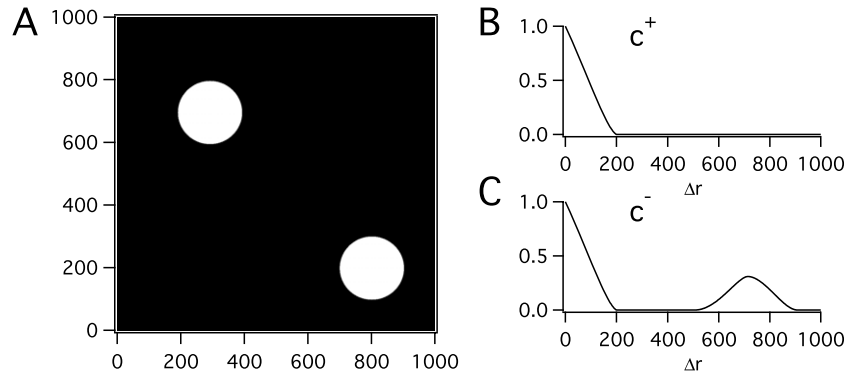


Figure 2. (A) Two circles of size $D = 200$ at a distance of $d = 707$ pixels. ((B), (C)) Radial correlation function $c^+(\Delta r, 0)$ and $c^-(\Delta r, 0)$ of panel A.

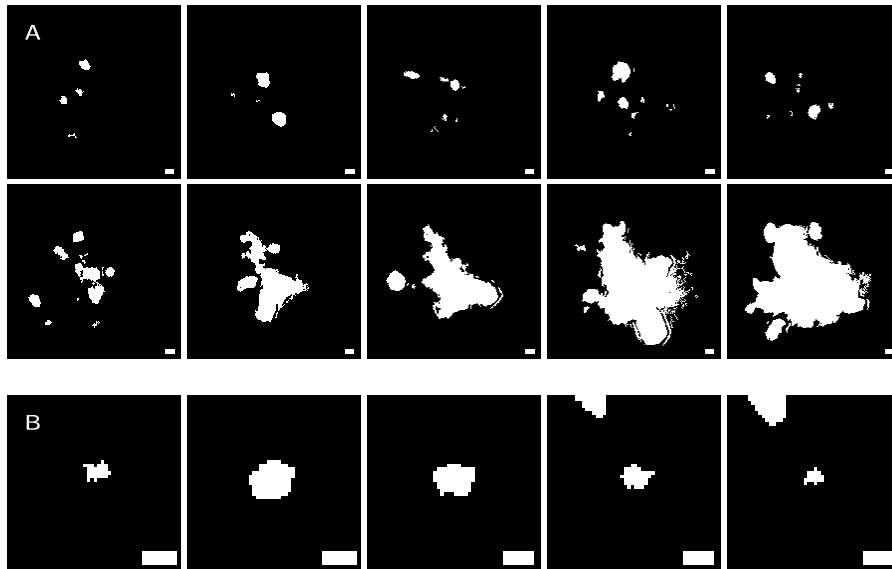


Figure 3. (A) Spreading cell with patches coming and going (movieA available at stacks.iop.org/JPhysCM/22/194106/mmedia). The time difference between snapshots is 50 s. (B) Time sequence of one single patch. The time difference between snapshots is 8 s. The scale bars show 1 μm in both panels.

averaging of observed contact patterns. Thus, we considered only the angular-averaged correlation functions:

$$c^{+/-}(\Delta r, \Delta t) = \sum_{\varphi} c^{+/-}(\Delta x(\Delta r, \varphi), \Delta y(\Delta r, \varphi), \Delta t) \quad (3)$$

where the summation is restricted to the first (c^+) or second (c^-) quadrant, respectively.

In order to set the stage for a proper interpretation of results obtained from spreading data, we consider the spatial correlation function of the image shown in figure 2(A). The two angular-averaged correlation functions $c^{+/-}(\Delta r, 0)$ both show a linearly decaying peak at the origin, see figures 2(B) and (C). The root $c^{+/-}(D, 0) = 0$ characterizes the correlation length corresponding to the diameter D of the two full circles in figure 2(A). The correlation function $c^-(\Delta r, 0)$ shows a second peak at $\Delta r = d$ corresponding to the radial distance d between the two circles. There is no such peak in $c^+(\Delta r, 0)$, since there is no other circle to the upper right or lower left of both circles. We take the mean correlation function corresponding

to the full dataset, $c = (c^+ + c^-)/2$, as the nominal correlation value. The difference $\Delta c = c^+ - c^-$ serves as an estimate of the experimental error in obtaining a proper average of the statistical ensemble.

3. Results

3.1. Early cell spreading

We find early cell spreading in fibroblasts to be characterized by adhesion patches with a typical distribution of sizes and lifetimes. In figure 3(A), we show a time lapse sequence of a spreading cell. A number of patches can be seen to appear and disappear as time progresses; see figure 3(B), for a magnified sequence of one patch. Finally, these patches fuse and the cell starts to extend onto the substrate. Thus, we identify this fusion event as the beginning of the basal phase (P0) of early spreading [7].

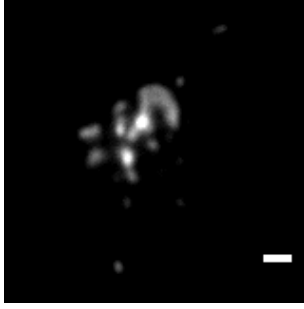


Figure 4. TIRF micrograph of a spreading cell just after fusion of the first few patches. The scale bar corresponds to $1 \mu\text{m}$.

The whole movie is available as supplemental material (available at stacks.iop.org/JPhysCM/22/194106/mmedia) in an original (movieAorig) and thresholded (movieAthresh) version along with three other examples (movieB, movieC and movieD).

Quantitative confirmation that patches seen with RICM correspond to cell areas in close contact with the substrate was obtained from TIRF micrographs of spreading cells. In figure 4, we show a cell shortly after initiation of patch fusion. Bright patches of the fluorophore-labeled cell membrane can be clearly seen. The TIRF decay length was set to $d_\lambda = 68 \text{ nm}$. Thus, membrane patches were indeed very close to the substrate.

We calculated normalized correlation functions from the thresholded and inverted movies including all frames up to the fusion point. In figure 5, we show a typical example, along with spatial ($\Delta t = 0$) and temporal ($\Delta r = 0$) cuts. Clearly, there is a well-defined correlation length D_0 and time τ_0 , which we nominally determine from the points closest to the origin

where the correlation drops below a value of 0.05. In figure 6, the data distribution of correlation length and time, i.e. size and lifetime of patches, respectively, is shown. The spatial cut exhibits a shoulder corresponding to the mean distance between patches.

Close inspection of single adhesion patches reveals that birth and death events of these patterns are asymmetric. Whereas patches appear rather quickly, it takes them considerably more time to disappear. In figure 7, we show the area-equivalent diameter $D_A = 2\sqrt{A/\pi}$ as a function of time for a few examples representing single patch dynamics; compare figure 3(B).

3.2. Time-dependent correlation functions

There is a pronounced change in the adhesion pattern at the point of fusion of the first two patches. One might expect that there is an effect at even earlier times. This should be visible in a time-dependent correlation function. Up to now, we have disregarded such a possibility by averaging over the whole movie well prior to fusion of patches. In order to catch a time dependence of the correlation function, we cut the movies into partitions of varying length and phase shift with respect to the start of recording. Indeed, as shown in figure 8, we find a strong change in the correlations with time, especially around the point of fusion. The behaviour in space and time is somewhat different. However, both the temporal and spatial cut of the correlation function show a pronounced change at the point of fusion, albeit at slightly different time points.

Following our concept to interpret pronounced changes in the characteristics of cell spreading as dynamic phase transitions [2], we want to test whether any changes found are occurring spontaneously or continuously in time. To this end,

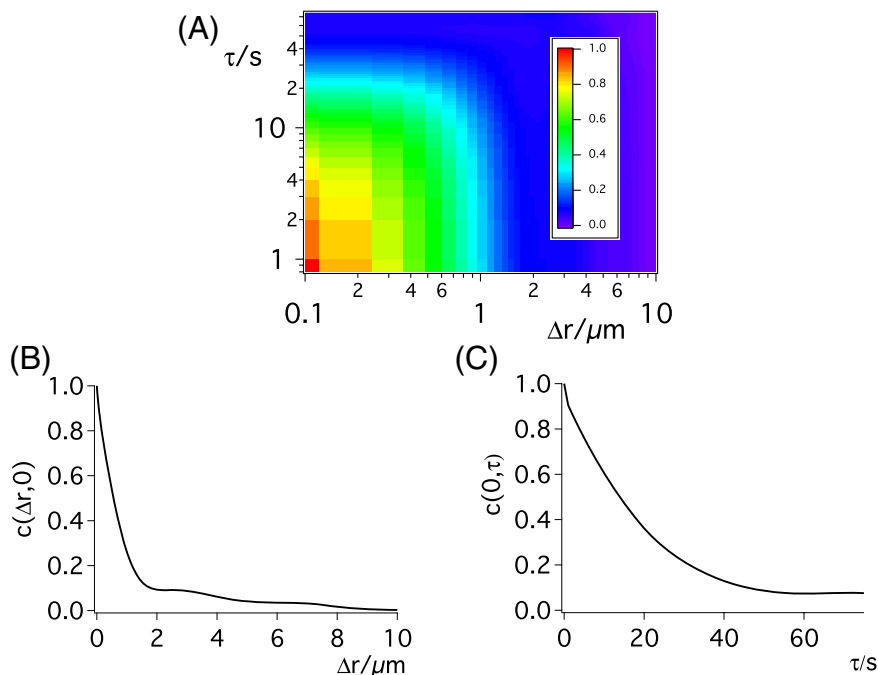


Figure 5. Correlation function of a spreading cell prior to patch fusion: (A) spatio-temporal color-coded map and (B) spatial cut: the correlation decay corresponds to an average patch size of $1 \mu\text{m}$. Note the flat shoulder around $\Delta r = 2.6 \mu\text{m}$ corresponding to the nearest-neighbour distance. (C) Temporal cut: the correlation decay corresponds to an average patch lifetime of 30 s.

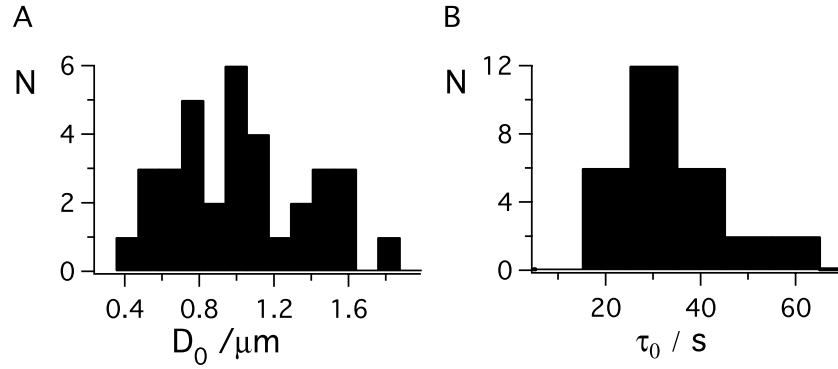


Figure 6. Histograms of patch size (A) and lifetime (B). In order to reveal patch variability, histograms were obtained from cropped movie sequences of single patches.

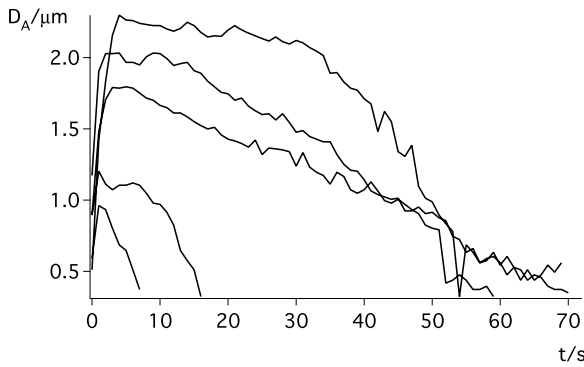


Figure 7. Time sequences of area-equivalent diameter showing the birth and death of single patches. Note that it is the time average of these curves which gives rise to the histogram in figure 6.

we need to pinpoint the exact location of the transition and distinguish between a possible jump and continuous changes in the shape of the correlation function at the transition. From the very nature of the fusion event, one would expect a jump in the typical size of the patches. However, different patches might fuse at slightly different points in time, leading to a somewhat smeared-out transition. Indeed, that is what we find. In order to characterize the spatial correlation functions shown in figure 8, we determine the correlation length R_c defined via $c(R_c, 0) = 1/2$. We have done this for a number of different partitions as shown in figure 9. There is a clear step-like transition visible.

Let us pause for a moment and note that the calculation of correlation functions of the movie partitions corresponds to box averaging our dataset. Consider our expectation when applying this procedure to a function with a jump versus a continuous ramp in between constant values. For any given size of the individual movie partitions, a jump is smeared out in a ramp with a width equal to the partition size, all different values of the ramp being assumed when the phase of the partition is shifted continuously. For a genuine ramp in the data this is different. For large partitions, we get the same result. However, as soon as the partition size drops below the size of the ramp in the raw data, the slope of the ramp obtained from averaging the data is not changing any more as a function of partition size but approaches the slope of the raw data ramp.

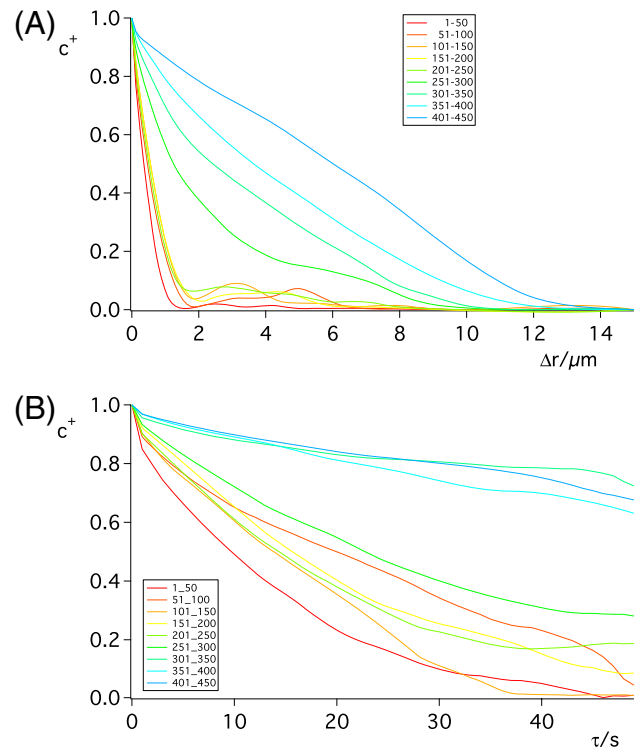


Figure 8. Time-dependent spatial (A) and temporal (B) correlation functions of a spreading cell including the fusion point. The partition size is 50 s as indicated.

In figure 9, we show one result for such a procedure. As expected, the slopes at the fusion point are decreasing with partition size up to a minimal size of 25 s, i.e. frames, at which the slope becomes independent of partition size. Thus, further analysis should proceed with this partition size. However, at the fusion point correlation times assume values of approximately 50 s^3 and become larger beyond. Moreover, the slope for the partition size 50 s is already rather close to the asymptotic value. Therefore, we chose this size as an appropriate compromise between temporal resolution and the necessary data size for one measurement of the correlation function with moderate statistical fluctuations.

³ This means that patches do not appear and disappear at smaller time intervals.

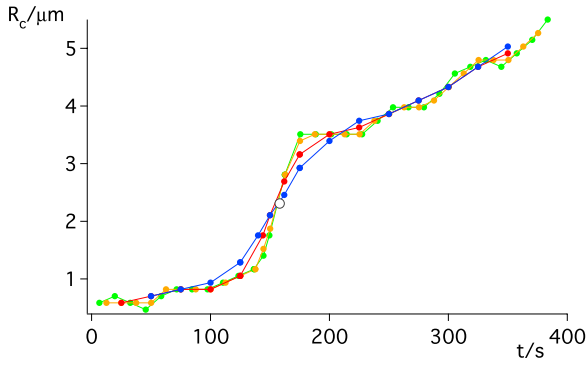


Figure 9. Correlation length R_c^+ obtained from c^+ with several different partition sizes (blue 100 s, red 50 s, yellow 25 s, green 13 s: from bottom to top at $t = 175$ s) for one cell as a function of time. The point of fusion is indicated by an open circle.

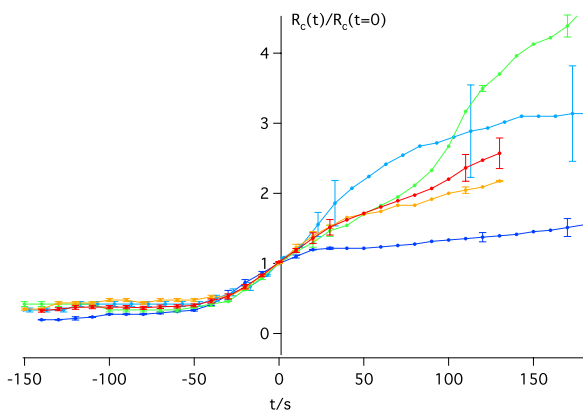


Figure 10. Master curve of correlation length: correlation lengths R_c^+ and R_c^- were obtained from c^+ and c^- , respectively, and averaged. The average $R_c = (R_c^+ + R_c^-)/2$ from four different cells is shown. Correlation lengths were shifted in time relative to the fusion point ($t = 0$) and scaled to unity. Scaling factors were $1.4 \mu\text{m}$ (movieA, green; movieD, light blue, available at stacks.iop.org/JPhysCM/22/194106/mmedia), $1.3 \mu\text{m}$ (movieB, yellow, available at stacks.iop.org/JPhysCM/22/194106/mmedia) and $3.0 \mu\text{m}$ (movieC, blue, available at stacks.iop.org/JPhysCM/22/194106/mmedia). The average master curve is shown in red. The error bars correspond to $\Delta R_c = R_c^+ - R_c^-$. Note that the large error bars in one cell (light blue) originate in a strongly non-spherical cell body after fusion.

We define the fusion point as the intersection between spatial correlation curves corresponding to different partition sizes. If there are several intersections, we take the average of those intersections near the sigmoidal midpoint of the transition. We shift the fusion points of different movies into the origin and scale the correlation length at the fusion point to unity. Using this scaling procedure, we obtain a master curve in the vicinity of the fusion point as shown in figure 10. The master curve has a slope of 1 min^{-1} corresponding to a relative growth of 100% of the correlation length per minute at the transition. The error bars on the correlation functions, i.e. $\Delta c = c^+ - c^-$, have a somewhat different meaning depending whether cells have reached their patch fusion points or not. Prior to fusion, the error bars reflect the statistical error from averaging several patch regions of the cell. After fusion, the

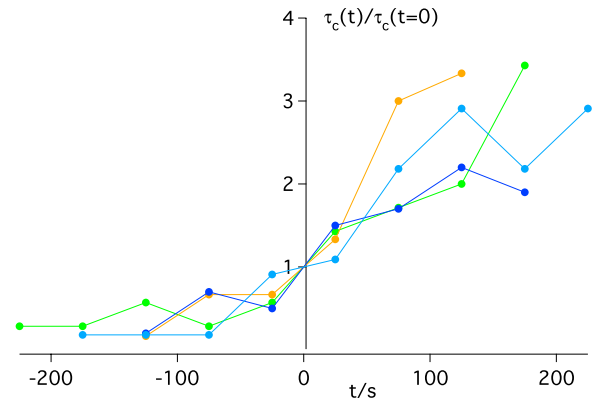


Figure 11. Master curve of correlation time: correlation times τ_c from four different cells are shown. Correlation times were shifted in time relative to the fusion point ($t = 0$) and scaled to unity. Scaling factors were 3.5 s (movieA, green, available at stacks.iop.org/JPhysCM/22/194106/mmedia), 6.0 s (movieB, yellow, available at stacks.iop.org/JPhysCM/22/194106/mmedia), 10 s (movieC, blue, available at stacks.iop.org/JPhysCM/22/194106/mmedia) and 5.5 s (movieD, light blue, available at stacks.iop.org/JPhysCM/22/194106/mmedia).

main cell body is dominating the correlation function and Δc gives an estimate of the degree of anisotropy of cell spreading.

Temporal correlations are characterized via the correlation time τ_c defined from $c(0, \tau_c) = 0.9^4$. In figure 11, we show the time dependence of the correlation times relative to the fusion points. We use the same fusion points as determined above from the spatial correlation functions. Correlation times are scaled to unity at the fusion point as well. Again, we find a similar relative increase for different cells around the fusion point like we did for the spatial correlations. Scaling for the temporal correlations is not as evident as for spatial correlations. Nevertheless, the overall time dependence exhibits similar behavior. We find a relative increase of the correlation time between 20 and 100% per 50 s.

Correlation functions are calculated from the contact areas of a spreading cell including fused patches and the final cell body which dominate the growth of the correlation length. We were also interested in the growth behavior of the patches alone before and after the first fusion event. In order to achieve this, we have calculated correlation lengths of all single patches excluding correlations with neighbouring patches and/or the cell body, see figure 12. Correlation lengths are plotted as a function of the time of the respective patch in the movie, i.e. time points for each patch are calculated as the mean of birth and death times of the respective patch. Underneath the strong spatial fluctuations among patches, we find a weak increase over time for the correlation length of the patches. We have calculated linear fits with and without the last patch. Excluding the last patch, there is still a marginally significant non-zero positive slope of $(75 \pm 75) \text{ nm s}^{-1}$ with a confidence interval of 95%.

⁴ We calculated τ_c instead of τ_0 , since temporal correlations do not drop to zero after the fusion point for the time windows considered.

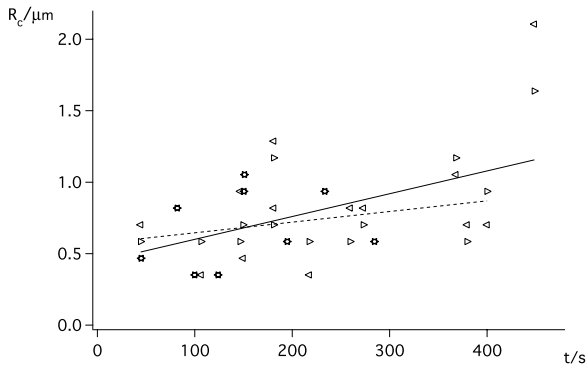


Figure 12. Single patch correlation length $R_c^{+/-}$ as a function of time. Time points for each patch are calculated as the mean of birth and death times of the respective patch. Open triangles with different orientations correspond to correlation length determined from c^+ and c^- , respectively. Linear fits with (solid line) and without (dashed line) the last patch are shown.

4. Discussion

We have found cell spreading in mouse embryonic fibroblasts to commence with a tiptoeing mode where the cell makes transient contact to the substrate via membrane patches with a typical size and lifetime. Similar behavior was reported by Pierres *et al* [21] for monocytic THP-1 cells which develop mostly permanent contacts. These growing patches are preceded by the accumulation of actin at sites of future contacts. This finding points to an active process. Likewise, our observation of dynamic transient patches seems to imply active retraction of the plasma membrane from the substrate. We interpret this mode as a new phase of cell motility [5] preceding the basal phase of cell spreading [2, 7]. We find the transition between this tiptoeing phase and the basal phase to be characterized by master curves for spatial and temporal correlations.

We believe that a description of cell motility with phases and dynamic phase transitions is not only imposing a formal classification scheme but reflects underlying protein modules [24] which in fact do undergo transition between different functional states. These protein modules constitute a hierarchical structure. Within the hierarchical phase model of cell motility we conceptually consider three system levels. First, the phase building blocks, i.e. the physical constituents of the basic cell motility apparatus and their interactions; second, the phase parameters, i.e. the phase controlling proteins; and third, the phase trajectories, i.e. the sequence of functional states regulated by global cellular networks. It is on the latter system level where interactions among different modules regulating diverse functions take place. This conceptual approach allows us to disentangle physical mechanisms from biological regulation.

One of the key questions is whether cell spreading is an active process throughout or in parts passively controlled by the properties of cellular soft matter. Undoubtedly, the formation of contracting lamellipodia and focal adhesions in late spreading is an active process. However, there is some recent evidence that the continuous spreading phase is

governed by a balance between the gain in adhesion energy and the viscous dissipation in the cytoskeleton. Cuvelier *et al* [20] find a power-law behavior consistent with such a mechanism. They propose a scaling exponent $1/2$ for the time dependence of the adhesion area $A(t) \sim t^{1/2}$. Indeed, we had found such an exponent for a subpopulation of spreading cells [2]. However, there is at least one more population with a faster area growth discriminated by the relative area growth during the continuous spreading phase. Interestingly, we find a master curve for this quantity at the transition into the basal phase. It will be exciting to see whether there is a connection. Cuvelier *et al* treat the basal phase as a simple lag time for cell spreading. In contrast, we found adhesion area growth already during the basal phase. We note in passing that the plasma membrane area during spreading is not constant but rather increases due to exocytotic events [25]. This complicates analysis further. Moreover, we have shown in this work that there is even another phase, the tiptoeing phase, prior to the basal phase. Whether the transition between these two phase is actively regulated or rather passive remains to be further investigated. A particular example for a passive process is the crossover between two scaling regimes as proposed to arise within the continuous spreading phase when the effective volume within which dissipation occurs changes with cellular shape [20]. What would be the difference to an actively controlled dynamic phase transition? In both cases, one sees a change of the dynamic behavior with time. However, in contrast to a scaling crossover, a dynamic phase transition is caused by a (possibly abrupt) change in a parameter controlling the motile state of the cell. In turn, changes in such a control parameter are regulated by the signaling network of cell spreading. As argued above, we conjecture the transition between the tiptoeing phase and the basal phase to be controlled by the active actin gel. In general, there will be a mixture between passive processes and active control in the cell. One mechanism of spreading does not exclude the other. All system levels, i.e., the physical constituents of the basic cell motility apparatus and their interactions, their locally controlling proteins, as well as globally regulating networks will work together to ensure a proper functional state of the mobile cell.

References

- [1] Ridley A J, Schwartz M A, Burridge K, Firtel R A, Ginsberg M H, Borisy G, Parsons J T and Horwitz A R 2003 Cell migration: integrating signals from front to back *Science* **302** 1704–9
- [2] Döbereiner H-G, Dubin-Thaler B, Giannone G and Sheetz M P 2004 Dynamic phase transitions in cell spreading *Phys. Rev. Lett.* **93** 108105
- [3] Dubin-Thaler B J, Giannone G, Döbereiner H-G and Sheetz M P 2004 Nanometer analysis of cell spreading on matrix-coated surfaces reveals two distinct cell states and STEPs *Biophys. J.* **86** 1794–806
- [4] Betz T, Lim D and Käs J A 2006 Neuronal growth: a bistable stochastic process *Phys. Rev. Lett.* **96** 098103
- [5] Döbereiner H-G, Dubin-Thaler B J, Hofman J M, Xenias H S, Sims T N, Giannone G, Dustin M L, Wiggins C H and Sheetz M P 2006 Lateral membrane waves constitute a universal dynamic pattern of motile cells *Phys. Rev. Lett.* **97** 38102
- [6] Shlomovitz R and Gov N S 2007 Membrane waves driven by actin and myosin *Phys. Rev. Lett.* **98** 168103

- [7] Dubin-Thaler B J, Hofman J M, Cai Y, Xenias H, Spielman I, Shneidman A V, David L A, Döbereiner H-G, Wiggins C H and Sheetz M P 2008 Quantification of cell edge velocities and traction forces reveals distinct motility modules during cell spreading *PLoS ONE* **3** e3735
- [8] Machacek M and Danuser G 2006 Morphodynamic profiling of protrusion phenotypes *Biophys. J.* **90** 1439–52
- [9] Geiger B, Bershadsky A, Pankov R and Yamada KM 2001 Transmembrane extracellular matrix-cytoskeleton crosstalk *Nat. Rev. Mol. Cell. Biol.* **2** 793–805
- [10] Giannone G, Dubin-Thaler B J, Rossier O, Cai Y, Chaga O, Jiang G, Beaver W, Döbereiner H-G, Freund Y, Borisy G and Sheetz M P 2007 Lamellipodial actin mechanically links myosin activity with adhesion-site formation *Cell* **128** 561–75
- [11] Döbereiner H-G *et al* 2005 Force sensing and generation in cell phases: analyses of complex functions *J. Appl. Physiol.* **98** 1542–6
- [12] Sawada Y, Tamada M, Dubin-Thaler B J, Cherniavskaya O, Sakai R, Tanaka S and Sheetz M P 2006 Force sensing by mechanical extension of the Src family kinase substrate p130Cas *Cell* **127** 1015–26
- [13] Vogel V and Sheetz M 2006 Local force and geometry sensing regulate cell functions *Nat. Rev. Mol. Cell Biol.* **7** 265–75
- [14] Bershadsky A, Kozlov M and Geiger B 2006 Adhesion-mediated mechanosensitivity: a time to experiment, and a time to theorize *Curr. Opin. Cell Biol.* **18** 472–81
- [15] Bischofs I B, Schmidt S S and Schwarz U S 2009 Effect of adhesion geometry and rigidity on cellular force distributions *Phys. Rev. Lett.* **103** 048101
- [16] Smith A-S and Sackmann E 2009 Progress in mimetic studies of cell adhesion and the mechanosensing *Chem. Phys. Chem.* **10** 66–78
- [17] Sengupta K, Aranda-Espinoza H, Smith L, Janmey P and Hammer D 2006 Spreading of neutrophils: from activation to migration *Biophys. J.* **91** 4638–48
- [18] Cohen M, Kam Z, Addadi L and Geiger B 2006 Dynamic study of the transition from hyaluronan to integrin-mediated adhesion in chondrocytes *EMBO J.* **25** 302–11
- [19] Cohen M, Joester D, Sabanay I, Addadi L and Geiger N 2007 Hyaluronan in the pericellular coat: an additional layer of complexity in early cell adhesion events *Soft Matter* **3** 327–32
- [20] Cuvelier D, They M, Chu Y S, Dufour S, Thiery J P, Bornens M, Nassoy P and Mahadevan L 2007 The universal dynamics of cell spreading *Curr. Biol.* **17** 694–9
- [21] Pierres A, Benoliel A-M, Touchard D and Bongrand P 2008 How cells tiptoe on adhesive surfaces before sticking *Biophys. J.* **94** 4114–22
- [22] Su J, Muranjan M and Sap J 1999 Receptor protein tyrosine phosphatase activates Src-family kinases and controls integrin-mediated responses in fibroblasts *Curr. Biol.* **9** 505–11
- [23] Pedrotti F, Pedrotti L, Bausch W and Schmidt H 2002 *Optik für Ingenieure—Grundlagen* (Berlin: Springer)
- [24] Hartwell L H, Hopfield J J, Leibler S and Murray A W 1999 From molecular to modular cell biology *Nature* **402** C47–52
- [25] Gauthier N C, Rossier O M, Mathur A, Hone J C and Sheetz M P 2009 Plasma membrane area increases with spread area by exocytosis of a GPI-anchored protein compartment *Mol. Biol. Cell* **20** 3261–72